Center Frequency and Bandwidth Controllable Microstrip Bandpass Filter Design Using Loop-Shaped Dual-Mode Resonator

Hsuan-Ju Tsai, *Student Member, IEEE,* Nan-Wei Chen, *Member, IEEE*, and Shyh-Kang Jeng

***Abstract*—A design approach for developing microwave bandpass filters (BPFs) with continuous control of the center frequency and bandwidth is presented. The proposed approach exploits a simple loop-shaped dual-mode resonator that is tapped and perturbed with varactor diodes to realize center frequency tunability and passband reconfigurabilty. The even- and odd-mode resonances of the resonator can be predominately controlled via the incorporated varactors, and the passband response reconfiguration is obtained with the proposed tunable external coupling mechanism, which resolves the return losses degradation attributed to conventional fixed external coupling mechanisms. The demonstrated approach leads to a relatively simple synthesis of the microwave BPF with an up to 33% center frequency tuning range, an excellent bandwidth tuning capability, as well as a high filter response reconfigurability, including an all-reject response.**

***Index Terms*—Bandpass filter (BPF), dual mode, reconfigurable filter, tunable filter, varactor diode.**

I. Introduction

FUTURE communication systems, such as cognitive and software-defined radio [1], [2], call for the development of microwave components with controllable characteristics. Specifically, these components, including power amplifiers with adaptive output networks [3], [4], tunable antennas [5], tunable low-pass filters [6], and tunable bandpass filters (BPFs) [7]–[32], are designed to operate at different frequency bands with varied bandwidth, and the system architecture is, therefore, able to be altered for improvement on data connectivity and throughput. Among components of this kind, the planar reconfigurable/tunable BPFs with adjustable fractional bandwidth or movable center frequency are considered as a candidate to replace the often-used switched filter banks. These filters are widely realized using reactive elements, including microelectromechanical system (MEMS) [7], [8], ferroelectric devices [9], [10], piezoelectric transducers (PETs) [11], [12], p-i-n diodes [13]–[17], varactor diodes [18]–[30], etc., with element values varied in a continuous or discrete manner. According to passband characteristics, planar reconfigurable/tunable BPFs can be categorized into three types, which are: 1) Type I: passband with a fixed center frequency and a controllable bandwidth [15]–[18]; 2) Type II: passband with a tunable center frequency and a constant bandwidth [7]–[14], [19]–[24]; and 3) Type III: passband with a tunable center frequency as well as a controllable bandwidth [25]–[31]. The previous works on each filter type are briefly reviewed as follows.

The p-i-n diode incorporated ring resonator with a switchable number of transmission poles [15], varactor-tuned open/short transmission-line structures with separately relocatable transmission zeros [18], or p-i-n diode incorporated switched coupled lines with three-state bandwidth tuning [17] was adopted for the design of the Type-I filter with bandwidth reconfigurability. As for the Type-II filters, the filter of a fixed bandwidth was realized with varactor-tuned microstrip comblines loaded with lumped series LC resonant circuits [19], and the constant bandwidth is attributed to the controllable slope parameter. In [14], a parallel-coupled switched delay lines were adopted for high power handling and excellent linearity. However, additional wideband power splitters render the entire filter bulky. Other approaches, including the dual-mode ring resonator perturbed using meander lines together with varactors [20] and the dual-mode open loop resonator loaded with varactors [21], were exploited for center-frequency tunability via a control of the mode coupling. On the other hand, [22] and [23], respectively, present the schemes based on independent and mixed electric and magnetic coupling among varactor-tuned microstrip transmission-line resonators to obtain the center-frequency tunability. To obtain both center-frequency and bandwidth tuning capability, Type-III filters were developed with the structures, such as the so-called coupling reducer introduced between microstrip comblines [25], the varactor-tuned comblines [26], and the resonator with a controllable slope parameter [27], to provide an additional degree of freedom of bandwidth adjustment. Recent techniques, including the dual-mode triangular patch resonance altered with varactors [28] and the microstrip dual-mode ring resonance perturbed with varactors [29], were reported for filter realization. Technically, the dual-mode ring resonator, known for its high selectivity, dual-mode resonance for compactness [21], as well as easy extension to multistage filter designs [30], [32], was first proposed by Wolff [33]. It was shown that the degenerate modes of a ring resonator are excited with a perturbation element to introduce two transmission zeros at two passband edges of a microstrip BPF [34]. In addition,

Manuscript received April 23, 2013; revised August 16, 2013; accepted August 19, 2013. Date of publication September 10, 2013; date of current version October 02, 2013. This work was supported in part by the National Science Council of Taiwan under Contract NSC 102-2221-E155-016 and Contract and NSC 102-2218-E155-001.

H.-J. Tsai and S.-K. Jeng are with the Department of Electrical Engineering and the Graduate Institute of Communication Engineering, National Taiwan University, Taipei 10617, Taiwan (e-mail: shamyah@hotmail.com; d99942003@ntu.edu.tw; skjeng@cc.ee.ntu.edu.tw).

N.-W. Chen is with the Department of Communications Engineering, Yuan Ze University, Jhongli 32003, Taiwan (e-mail: nwchen@saturn.yzu.edu.tw).

Digital Object Identifier 10.1109/TMTT.2013.2280129

0018-9480 © 2013 IEEE

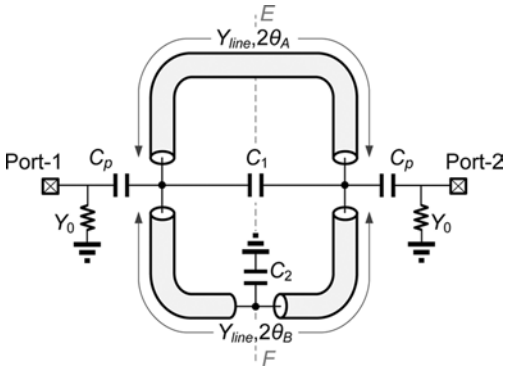

Fig. 1. Ideal circuit representation of the proposed dual-mode BPF.

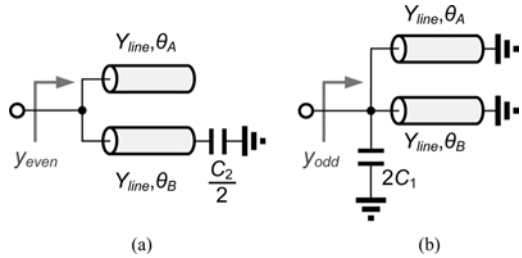

Fig. 2. Equivalent circuits of the dual-mode filter excluding the tapped capacitance C_p. (a) Even-mode circuit. (b) Odd-mode circuit.

the degenerate-mode coupling is investigated in [28] through a coupling matrix analysis and the element-value extraction relies on a full-wave simulator. In [29], the even- and odd-mode resonances of a ring resonator are perturbed with diagonally incorporated shunt varactors to achieve center-frequency tunability together with a controllable bandwidth. However, the determination of the tapped capacitance associated with the filter response is not described.

Compared to the filter synthesis reported in [29], a more effective and complete circuit-aided design approach of the BPF using the varactor tapped and perturbed dual-mode resonator is presented. Two essential improvements regarding filter synthesis and reconfiguring capability are outlined as follows. First, the decision of the tapped capacitor is included for a more robust filter analysis since the tapped capacitor affects the dual-mode resonances when the resonator is not weakly coupled. In addition, the authors present a passband response reconfiguration, e.g., switching Butterworth response to a Chebyshev one with a specified ripple level, through an external coupling tuning via the tapped capacitor. The proposed tunable external coupling mechanism resolves the return losses (*RLs*) degradation obtained with the fixed external coupling one [28]. Here, the passband of the proposed BPF is able to be reconfigured to Chebyshev, Butterworth, quasi-elliptic, or a so-called "all-reject" response. The passband switch-off capability for a potential application in the time-division duplexing communication systems [35]. Second, the even/odd mode resonance is able to be separately relocated easily with an adjustment of the shape of the loop-shaped resonator, which leads to a high design freedom on the control of the dual-mode resonance.

This paper is organized as follows. Section II details the design and analysis of the filter based on the proposed loop-shaped resonator. The experimental verification and effectiveness demonstration of the proposed design approach are presented in Section III. Section IV draws the conclusions of this work and outlines the future works.

II. Filter Analysis and Synthesis

Fig. 1 depicts the ideal circuit representation of the proposed dual-mode filter. It is shown that the filter is developed with a loop-shaped resonator fed by tapped coupling capacitors C_p and perturbed with two capacitors (C_1 and C_2). In Fig. 1, $Y_{line} = 1/Z_{line}$ is the characteristic admittance of the transmission line in a loop configuration, Y_0 is the source/load admittance of the filter, and θ_A and θ_B denote the electrical lengths of one half of the upper and lower sections of the loop-shaped resonator, respectively. In what follows, the characterization of the dual-mode resonator using the equivalent circuit is detailed. Specifically, the resonator is first characterized without the consideration of tapped capacitor C_p at the input and output ports. The analysis of the entire filter comprising the loop-shaped resonator and C_p is then presented. The passband reconfigurabilty along with the center frequency tunability is then described.

A. Dual-Mode Resonator Without C_p

The symmetric circuit topology with respect to the line $\overline{EF}$ leads to the adoption of the even/odd-mode analysis for resonator characterization [29], [37], [38], and the corresponding even- and the odd-mode equivalent (half) circuits are shown in Fig. 2(a) and (b), respectively. That is, the employed resonator allows dual-mode resonance. It is straightforward to show that the even- and odd-mode resonant frequencies satisfy (1) and (2), respectively,

$$y_{even} = 0 \tag{1}$$

$$y_{odd} = 0. \tag{2}$$

In (1) and (2), y_{even} and y_{odd} represent the normalized input admittances with respect to Y_{line}. The normalized input even-mode admittance y_{even} of the circuit shown in Fig. 2(a) can be expressed as

$$y_{even} = j\frac{2(\tan\theta_A + \tan\theta_B) + b_2(1 - \tan\theta_A \tan\theta_B)}{2 - b_2 \tan\theta_B} \tag{3}$$

where $b_2 = \omega C_2 / Y_{line}$ denotes the normalized susceptance of the capacitor C_2 with respect to Y_{line}. With a substitution of (3) into (1), it is easy to show that the even-mode resonance occurs while

$$f_r^{even} = -Y_{line}\frac{\tan\theta_{tot}}{\pi C_2} \tag{4}$$

where

$$\theta_{tot} = \theta_A + \theta_B. \tag{5}$$

Note that the electrical lengths (θ_A and θ_B) are functions of frequency. Similarly, the normalized input admittance y_{odd} of the circuit shown in Fig. 2(b) is written as

$$y_{odd} = j\{2b_1 - (\cot\theta_A + \cot\theta_B)\} \tag{6}$$

where $b_1 = \omega C_1/Y_{line}$ denotes the normalized susceptance of the capacitor C_1. The odd-mode resonance condition is obtained via substituting (6) into (2). As a result,

$$f_r^{odd} = \frac{Y_{line}}{4\pi C_1}(\cot\theta_A + \cot\theta_B) = \frac{Y_{line}}{4\pi C_1}\left\{\cot\left(\frac{\alpha}{1+\alpha}\theta_{tot}\right) + \cot\left(\frac{1}{1+\alpha}\theta_{tot}\right)\right\} \quad (7)$$

where the resonator form factor

$$\alpha = \frac{\theta_A}{\theta_B}. \quad (8)$$

Next, the controllable resonant characteristics of the dual-mode resonator attributed to variable C_1 and C_2 are described as follows.

1) The even- and odd-mode resonant frequencies, f_r^{even} and f_r^{odd}, can be separately adjusted by b_2 and b_1, i.e., C_2 and C_1.
2) It is shown in (4) that the even-mode resonant frequency f_r^{even} is determined with the θ_{tot} of the resonator regardless of α, i.e., the ratio of θ_A to θ_B, as defined in (8). In contrast, the odd-mode resonant frequency f_r^{odd} in (7) is associated with the ratio. Hence, with a given θ_{tot}, one has a design freedom on f_r^{odd}.
3) Considering the fundamental resonances ($\pi/2 \le \theta_{tot} \le \pi$), the tuning range of even- and odd-resonance modes can be deduced, respectively, from (4) and (7) as

$$\frac{1}{2t_p} \le f_r^{even} \le \frac{1}{t_p} \quad (9)$$

$$0 \le f_r^{odd} \le \frac{1}{t_p} \quad (10)$$

where t_p is the phase delay of the signal through the resonator. Consequently, the odd-mode tuning range is greater than the one of the even-mode resonance. That is to say, the perturbed capacitor attributed to the even-mode location appears to be the key component to the frequency tuning capability.

Fig. 3 numerically demonstrates the capability of relocating the even- and odd-mode resonances with respect to C_2 and C_1 at different θ_{tot} of three distinct α at 1 GHz when $Z_{line} = 95\,\Omega$. There are two observations on the adjustment of passband bandwidth, which is determined by the difference of the even- and odd-mode resonant frequencies. Firstly, in the case of $C_1 = C_2$, wider tuning range can be achieved in the low capacitance regime with a fixed loop circumference. In addition, the passband bandwidth is predominately determined by θ_{tot}, and the bandwidth increases as the ratio α approaches to unity. Specifically, as shown in Fig. 3(c), the case of $\alpha = 0.25$ (or $\alpha = 4$) inherits a relatively narrow bandwidth as compared to the case of $\alpha = 1$ when C_1 and C_2 are fixed at 5 pF. Secondly, in the case of different C_1 and C_2, the even- and odd-mode frequencies can be separately relocated with given θ_{tot} and α, which also results in a controllable filter bandwidth.

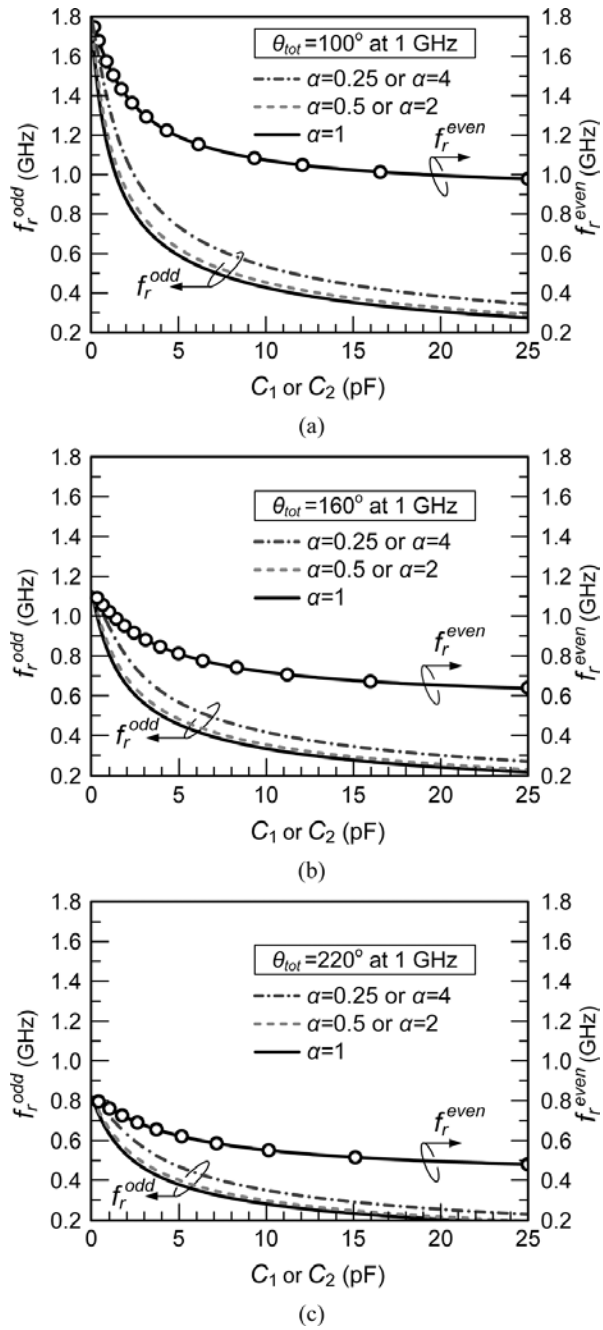

Fig. 3. Location of the even- and odd-mode frequencies f_r^{even} and f_r^{odd} with respect to the capacitance C_1 and C_2 with different α values when: (a) $\theta_{tot} = 100°$, (b) $\theta_{tot} = 160°$, and (c) $\theta_{tot} = 220°$, respectively, all at 1 GHz.

B. Dual-Mode Resonator With C_p—Proposed BPF

In Fig. 1, the capacitive coupling between the input/output port and the resonator is controlled by the tapped capacitances C_p. If the resonator is weakly coupled, i.e., C_p is small, the even- and odd-mode resonant frequencies of the entire filter are, respectively, approximated with (4) and (7), and the filter center frequency, f_c, is approximately equal to the average of f_r^{even} and f_r^{odd} [29], [37], [38]. As C_p is increased, the deviation of the even- and odd-mode resonant frequencies from (4) and (7) increases. Here, a relatively effective and accurate filter analysis with the inclusion of C_p is presented. Fig. 4(a) illustrates

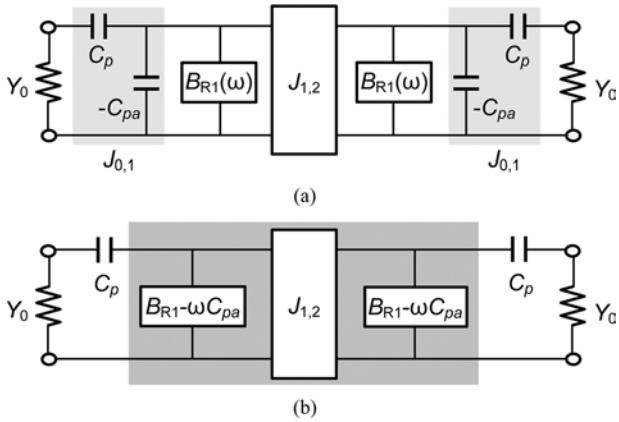

Fig. 4. (a) Symmetrical second-order capacitively coupled BPF topology. (b) Resulting circuit topology transformed from (a).

the circuit configuration of a second-order capacitively coupled filter topology in a symmetrical configuration. The capacitors C_p and C_{pa} are, respectively, parameterized as [39]

$$C_p = \frac{J_{0,1}}{2\pi f_c \sqrt{1-(J_{0,1})/{Y_0}^2}} \tag{11}$$

$$C_{pa} = \frac{C_p}{1+(2\pi f_c C_p/Y_0)^2}. \tag{12}$$

In (11), the admittance inverter $J_{0,1}$ is defined as

$$J_{0,1} = \sqrt{\frac{b_{r1}Y_0}{Q_{ext}}} = \sqrt{\frac{b_{r1}f_{bw}Y_0}{f_c g_0 g_1}} \tag{13}$$

where b_{r1} is the susceptance slope parameter of the shunt resonator $B_{\rm R1}$, f_{bw} is the passband width, $Q_{ext} = f_c g_0 g_1/f_{bw}$ is the external quality factor, and g_n is the nth element value of the conventional n-stage low-pass filter prototype [36].

By absorbing the distributed shunt negative capacitance $(-C_{pa})$ into the proximate resonator $B_{\rm R1}(\omega)$, the resulting circuit topology shown in Fig. 4(b) is related to the one presented in Fig. 1. Specifically, the dark gray region outlined in Fig. 4(b) is equivalent to loop-shaped resonator depicted in Fig. 1 in shunt with C_{pa}. Therefore, the corrected even- and odd-mode resonant frequencies, denoted as $\tilde{f}_r^{even}$ and $\tilde{f}_r^{odd}$, can be obtained by adding the shunt capacitor C_{pa} into the circuits in Fig. 2, and the resulting circuits are presented in Fig. 5. Similarly, the expressions associated with $\tilde{f}_r^{even}$ and $\tilde{f}_r^{odd}$ can be found with the manipulations presented in Section II-A. In contrast, the conditions for the even- and odd-mode resonances are, respectively, expressed as

$$\tilde{y}_{even} = y_{even} + jb_{pa} = 0 \tag{14}$$

$$\tilde{y}_{odd} = y_{odd} + jb_{pa} = 0 \tag{15}$$

where $\tilde{y}_{even}$ and $\tilde{y}_{odd}$ represent the corrected normalized input admittances with respect to Y_{line}, and $b_{pa} = \omega C_{pa}/Y_{line}$ is the normalized susceptance of C_{pa}. The relocations of $\tilde{f}_r^{even}$

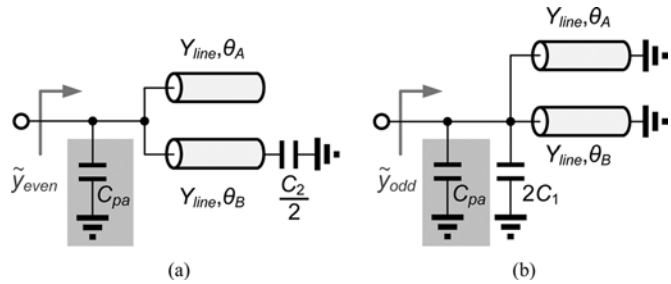

Fig. 5. Equivalent circuits of the loop-shaped resonator. (a) Even-mode circuit. (b) Odd-mode circuit.

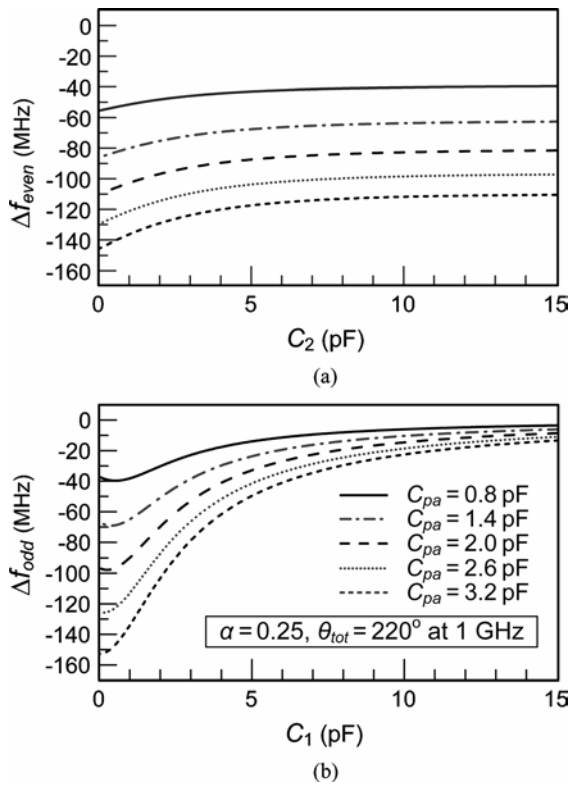

Fig. 6. Resonant frequency variations of the: (a) even-mode circuit and (b) odd-mode circuit.

and $\tilde{f}_r^{odd}$ due to capacitance C_{pa} can be implicitly expressed as follows:

$$\pi \tilde{f}_r^{even} C_2 = \frac{Y_{line}\left[\tan\left(\frac{1}{1+\alpha}\theta_{tot}\right)+\tan\left(\frac{\alpha}{1+\alpha}\theta_{tot}\right)\right]+2\pi \tilde{f}_r^{even} C_{pa}}{\tan\left(\frac{1}{1+\alpha}\theta_{tot}\right)\left[\tan\left(\frac{\alpha}{1+\alpha}\theta_{tot}\right)+2\pi \tilde{f}_r^{even} C_{pa}/Y_{line}\right]-1} \tag{16}$$

$$\pi \tilde{f}_r^{odd} C_1 = \frac{Y_{line}\left[\cot\left(\frac{1}{1+\alpha}\theta_{tot}\right)+\cot\left(\frac{\alpha}{1+\alpha}\theta_{tot}\right)\right]-2\pi \tilde{f}_r^{odd} C_{pa}}{2}. \tag{17}$$

Fig. 6 numerically shows the deviation of the even- and odd-mode resonant frequencies (i.e., $\Delta f_{even} = \tilde{f}_r^{even} - f_r^{even}$ and $\Delta f_{odd} = \tilde{f}_r^{odd} - f_r^{odd}$) with respect to C_{pa}, while $Z_{line} =$

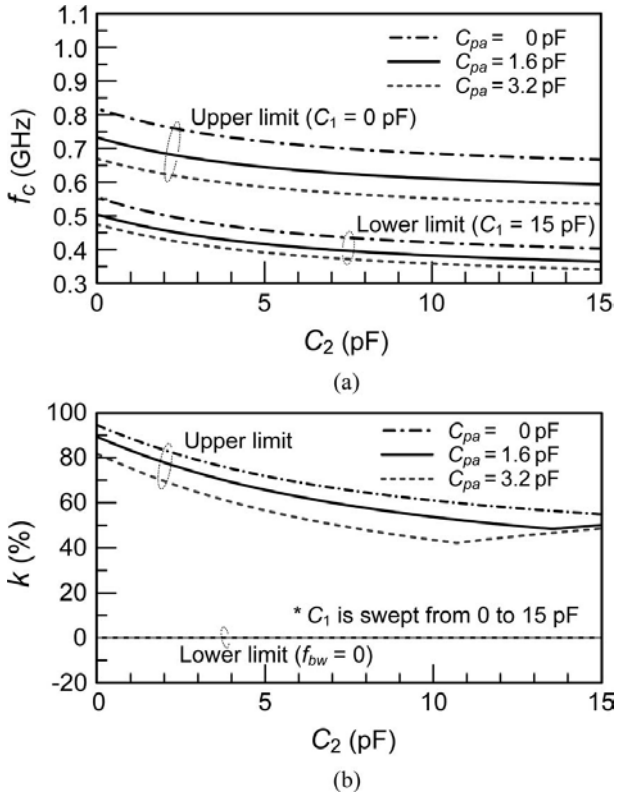

Fig. 7. Variations of the: (a) center frequency and (b) coupling coefficient with respect to C_2 as C_1 and C_{pa} vary ($Z_{line} = 95\ \Omega$, $\alpha = 0.25$, and $\theta_{tot} = 220°$ at 1 GHz).

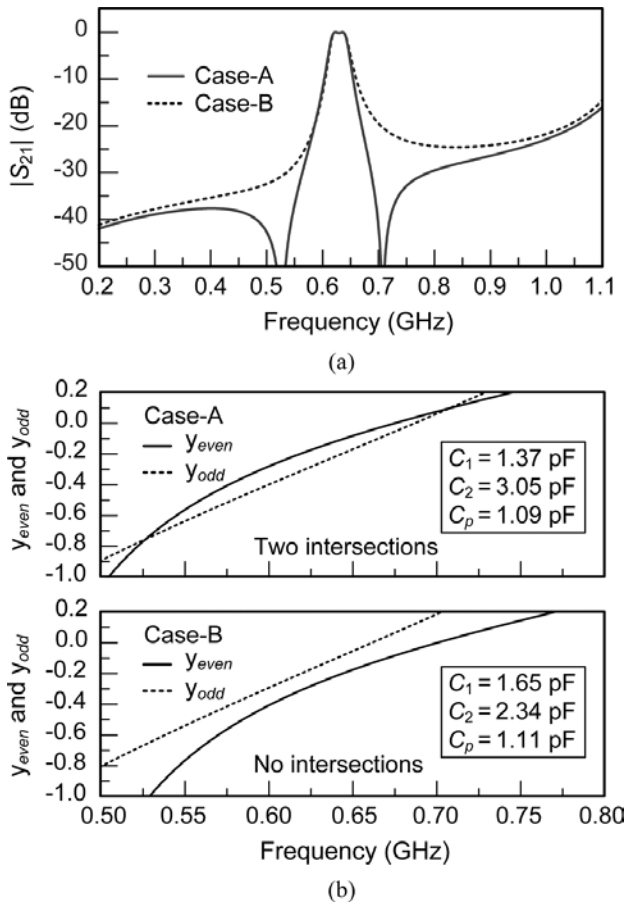

Fig. 8. (a) Transmission response with (Case-A)/without (Case-B) the transmission zeros and (b) corresponding y_{even} and y_{odd} while $Z_{line} = 95\ \Omega$, $\alpha = 0.25$, and $\theta_{tot} = 220°$ at 1 GHz.

$95\ \Omega, \alpha = 0.25$, and $\theta_{tot} = 220°$ at 1 GHz. As a result, the resonant frequencies decrease considerably as C_{pa} increases. That is, the tapped capacitor C_p is attributed to the frequency offset since C_{pa} is a function of C_p as described in (12). Next, the approximated formulas for estimating f_c and the mode coupling coefficient k between the even- and odd-mode resonances in terms of $\tilde{f}_r^{odd}$ and $\tilde{f}_r^{even}$ are written as

$$f_c = 0.5\left(\tilde{f}_r^{even} + \tilde{f}_r^{odd}\right) \tag{18}$$

and

$$k = \frac{2\left|\tilde{f}_r^{even} - \tilde{f}_r^{odd}\right|}{\tilde{f}_r^{even} + \tilde{f}_r^{odd}} = \frac{f_{bw}}{f_c\sqrt{g_1 g_2}}. \tag{19}$$

Fig. 7(a) and (b) presents the tuning capability of f_c and f_{bw} (in terms of k), respectively. With given C_2 and C_{pa}, the upper and lower limits of f_c are estimated by finding the maximum and minimum average values of $\tilde{f}_r^{even}$ and $\tilde{f}_r^{odd}$ as C_1 varies. In Fig. 8(a), the relatively large deviation of the upper limit of f_c is attributed to the large dual-mode resonance frequency offset with small C_1, as demonstrated in Fig. 6. The tuning range of f_c also becomes narrower as C_{pa} increases. As for the tuning range of k shown in Fig. 7(b), its upper and lower limits are estimated with given C_2 and C_{pa}, as well as the elemental values g_n for a given passband response when C_1 varies. As a result, the bandwidth tunability degrades when C_{pa} increases. Note that the zero bandwidth ($f_{bw} = 0$) occurs when $\tilde{f}_r^{even}$ equals $\tilde{f}_r^{odd}$, which indicates that the proposed filter is able to offer a so-called *all-reject* response presented later in Section III-C.

On the other hand, this dual-mode filter typically has two transmission zeros, and the transmission zeros appear when the transfer admittance $Y_{21} = ({Z_{ie}}^{-1} - {Z_{io}}^{-1})/2$ seen from the input/output port (see Fig. 1) attains to zero, where $Z_{ie} = (j\omega C_p)^{-1} + (\tilde{y}_{even}Y_{line})^{-1}$ and $Z_{io} = (j\omega C_p)^{-1} + (\tilde{y}_{odd}Y_{line})^{-1}$. As a result, the zero location is not affected by the tapped capacitance due to the cancellation of C_p terms, and the equation for locating the transmission zeros can be written as

$$y_{even} = y_{odd} \tag{20}$$

or

$$\frac{2(\mathrm{P}+\mathrm{T}) - 4b_1}{b_2(\mathrm{T} - 2b_1)} - \tan\left(\frac{1}{1+\alpha}\theta_{tot}\right) = 0 \tag{21}$$

where

$$\mathrm{P} = \tan\left(\frac{1}{1+\alpha}\theta_{tot}\right) + \cot\left(\frac{1}{1+\alpha}\theta_{tot}\right) \tag{22}$$

$$\mathrm{T} = \tan\left(\frac{\alpha}{1+\alpha}\theta_{tot}\right) + \cot\left(\frac{\alpha}{1+\alpha}\theta_{tot}\right). \tag{23}$$

The zero locations can be found via (21) by a conventional root-finding algorithm. Fig. 8(a) shows the filter responses with and without transmission zeros, viz. Cases-A and Case-B, respectively. The calculated y_{even} and y_{odd} against frequency for

TABLE I
FILTER PARAMETERS FOR DESIGN EXAMPLE

	Case-1	Case-2	Case-3	Case-4	Case-5
f_c (MHz)	450	450	530	610	610
f_{bw} (MHz)	25	25	25	25	50
RL (dB)	15	15	18	15	15
k (%)	7.14	7.14	7.05	5.27	10.54
Q_{ext}	16.75	16.75	16.09	22.71	11.36
Visible zeros	X	O	X	O	O
$\tilde{f}_r^{even}$ (MHz)	466.1	433.9	548.7	593.9	577.9
$\tilde{f}_r^{odd}$ (MHz)	433.9	466.1	511.3	626.1	642.1
C_p (pF)	2.250	2.013	2.049	1.341	1.964
C_1 (pF)	4.465	3.649	2.750	1.245	0.848
C_2 (pF)	10.003	15.270	4.800	3.631	3.585

both cases are presented in Fig. 8(b), where the top figure shows two intersections corresponding to the band-edge zero locations of Case-A.

C. Filter Synthesis

The design procedures for the proposed dual-mode filter are summarized as follows.

Step 1) Select $f_c = 0.5(\tilde{f}_r^{even} + \tilde{f}_r^{odd})$, f_{bw}, and the second-order low-pass prototype with elements $g_n (n = 0-3)$. Then calculate the related coupling coefficient k using (19). Once k is known, two solutions for the even- and odd-mode resonances ($\tilde{f}_r^{even} > \tilde{f}_r^{odd}$ and $\tilde{f}_r^{even} < \tilde{f}_r^{odd}$) can be specified.

Step 2) Specify Z_{line} and θ_{tot} with a designated α. The tapped capacitance C_p along with the perturbed capacitance C_2 and C_1 can be iteratively solved with in the order of (24), (13), (11), (12), (16), (17), and (19). Specifically, with an initial guess of C_{pa}, the slope parameter b_{r1} in (24) is calculated, and the admittance inverter $J_{0,1}$ in (13) is then obtained. Next, C_p in (11) is evaluated, and the convergence of C_{pa} is examined with the iterated C_{pa} using (12), the constraints on center frequency with (16) and (17), and the constraint on coupling coefficient k with (19). Meanwhile, C_1 and C_2 are determined with (16) and (17) once C_{pa} is converged,

$$b_{r1} = \frac{f_c Y_{line}}{4} \left. \frac{\partial \mathrm{Im}[\tilde{y}_{even}(f) + \tilde{y}_{odd}(f)]}{\partial f} \right|_{f=f_c}. \quad (24)$$

The above-described procedures are adopted to design a Chebyshev BPF of a tunable center frequency, controllable bandwidth, selectivity, and *RL* corresponding to the passband ripple for effectiveness demonstration. For clarity, only five controllable states are presented, the filter specifications and design parameters, such as C_p, C_1, and C_2, of each state are tabulated in Table I. The corresponding simulated S-parameter data are shown in Fig. 9. It is shown that $|S_{11}|$ remains almost unchanged while f_c and f_{bw} vary. As for the in-band $|S_{21}|$, the equi-ripple responses are observed for all states. Hence, the introduction of transmission zeros at both the lower and higher band edges significantly improves the selectivity, which results in a symmetrical frequency response.

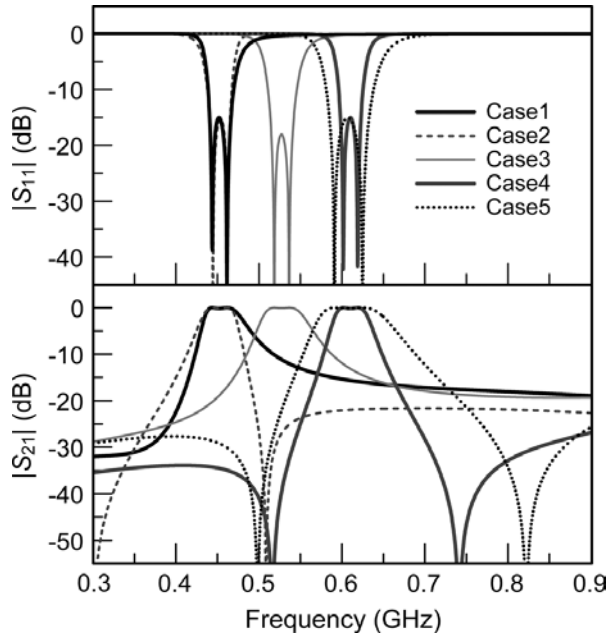

Fig. 9. Simulation S-parameters of the design example when $Y_0 = 0.02$ S, $Z_{line} = 95\ \Omega$, $\theta_A = 48°$, and $\theta_B = 172°$ ($\alpha = 0.28$, $\theta_{tot} = 220°$) at 1 GHz.

III. EXPERIMENTAL DEMONSTRATION AND VERIFICATION

Here, the design and realization of the demonstrated filter are described in Section III-A. The center frequency tunability and the bandwidth adjustment are shown in Section III-B. The passband reconfigurabilty is also demonstrated in Section III-C. Finally, the ability of switching the filter to an all-reject filter is presented. Here, all simulated results are obtained using the finite-element-based full-wave simulator, Ansoft HFSS, and the simulated results are verified with the measured ones.

A. Filter Design and Realization

The design parameters are selected as $Y_0 = 0.02$ S, $Z_{line} = 95\Omega$, $\theta_A = 48°$, and $\theta_B = 172°$, where both electrical lengths are at 1 GHz. The Chebyshev response of 0.14 dB ($RL = 15$ dB) passband ripple is specified with $g_0 = 1$, $g_1 = 0.9309$, $g_2 = 0.6495$, and $g_3 = 1.4332$. All the transmission-line sections (θ_A and θ_B in Fig. 1) are meandered and bended for filter compactness. Fig. 10(a)–(c) presents the detailed BPF layout, bias circuitry, and photograph of the fabricated filter. The filter is designed on a Rogers RO3006 substrate ($\epsilon_r = 6.15$, loss tangent 0.0025, and thickness 1.28 mm). All the varactors are employed in an antiseries configuration with a concern on varactor biasing, linearity, and power-handling capacity [24], [40], [41]. Specifically, the plastic packaged varactor diode SMV1413 of a series resistance 0.35 Ω and a varactor capacitance ranging from 1.77 to 9.24 pF when the reversal bias varies from 30 to 0 V [42] is selected to mimic the tapped capacitor C_p and the perturbed capacitor C_1. The varactor diode SMV1236 of a series resistance 0.5 Ω and a varactor capacitance ranging from 3.8

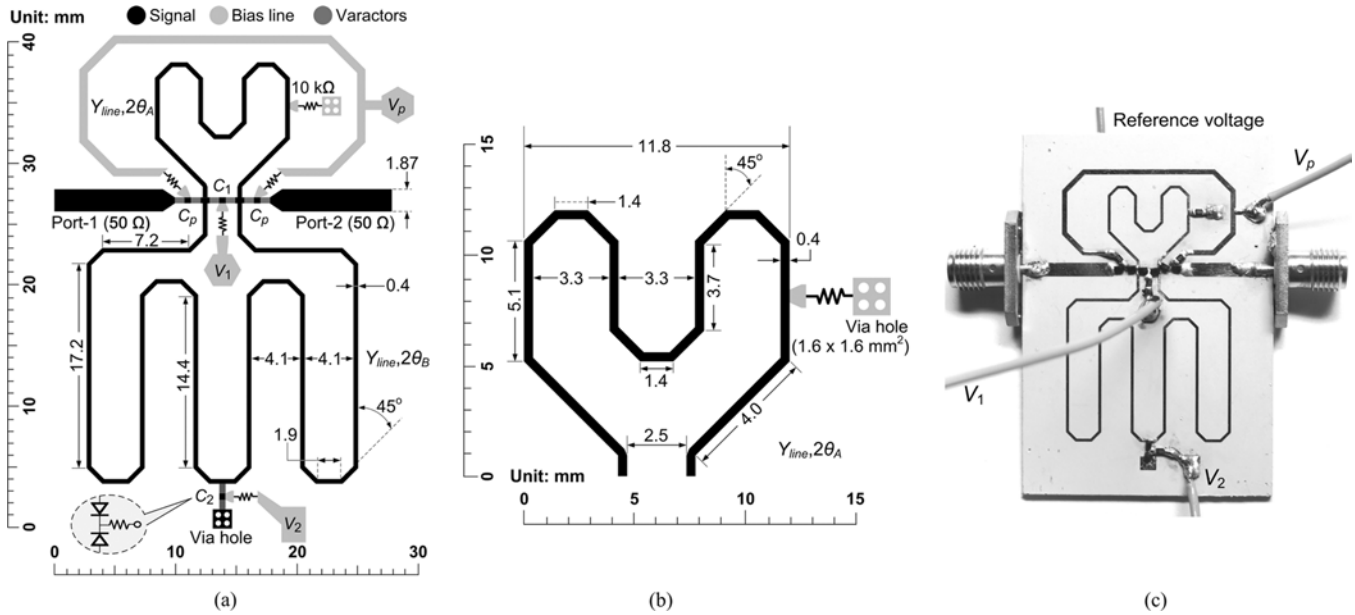

Fig. 10. (a) Configuration and dimensions of the demonstrated filter and (b) detailed layout of the upper arm structure ($2\theta_A$ at 1 GHz). (c) Photograph of the fabricated filter.

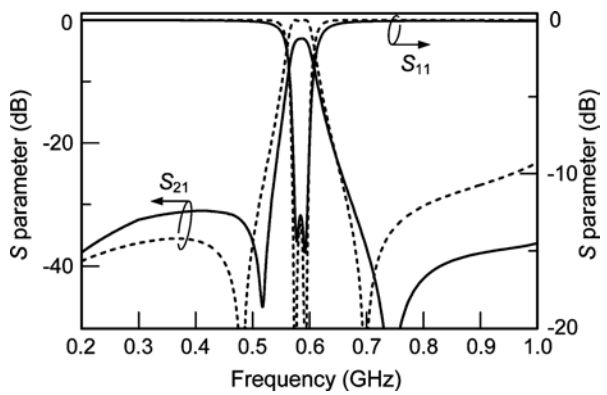

Fig. 11. Comparison of full-wave simulated results against circuit simulated results (solid: full-wave data; dashed: pure lossless circuit response).

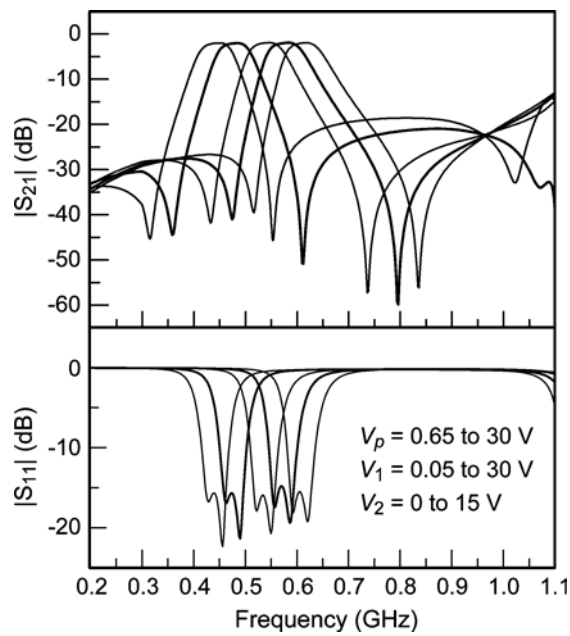

Fig. 12. Simulated S parameters with tunable frequency when passband ripple is specified as 0.14 dB.

to 26.75 pF when the reversal bias varies from 15 to 0 V [43] is chosen to realize C_2. The dc-to-RF isolation is achieved using five 10-kΩ lumped resistors connected in shunt with the antiseries varactors. Measurements on the filter are carried out with an Anritsu MS4623B vector network analyzer at small-signal levels (-15 dBm) to ensure varactor linearity. For varactor C_p, two bias tees manufactured by Woken Technology Inc. are directly applied at the input and output ports for dc biasing and blocking.

As for characterization, the entire filter is first simulated by the full-wave solver, Ansoft HFSS, with the matched (50 Ω) internal port setting at each varactor location. At this stage, the full-wave simulated results correspond to the S-parameter data of the filter characteristics including the transmission-line loss and transmission-line discontinuities, as well as bending inherited in the filter configuration. Next, the varactor coupling and perturbation are included and investigated using the commercial circuit solver, Agilent ADS 2011. Note the required voltages that corresponded to the antiseries varactors can be directly extracted using the conventional $ABCD$ matrix transformation (see [36, p. 13]). Fig. 11 shows the comparison of the circuit-aided full-wave simulation filter response against the pure lossless circuit (Fig. 1) synthesized response. As a result, the simulated in-band responses are in good agreement.

B. Center Frequency Tuning and Bandwidth Adjustment

Figs. 12 and 13 present the simulated and measured S-parameter data of the developed filter for demonstration of the center frequency tunability. The center frequency can be tuned from 430 to 600 MHz while the passband f_{bw} remains 40 MHz.

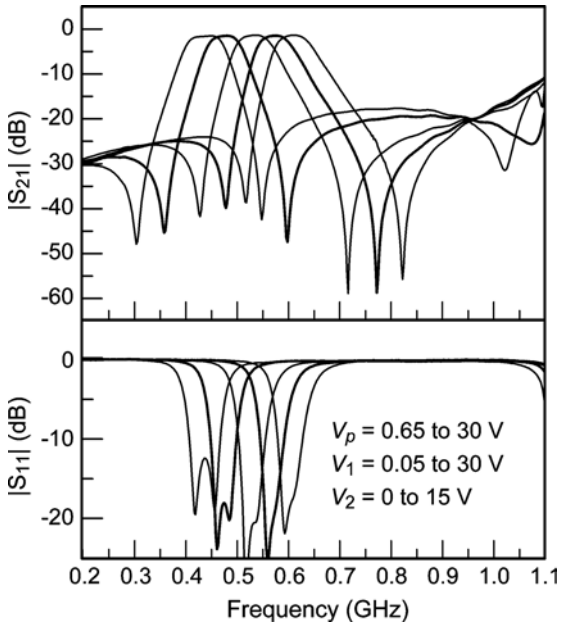

Fig. 13. Measured filter responses with tunable center frequency (f_{bw} = 40 MHz).

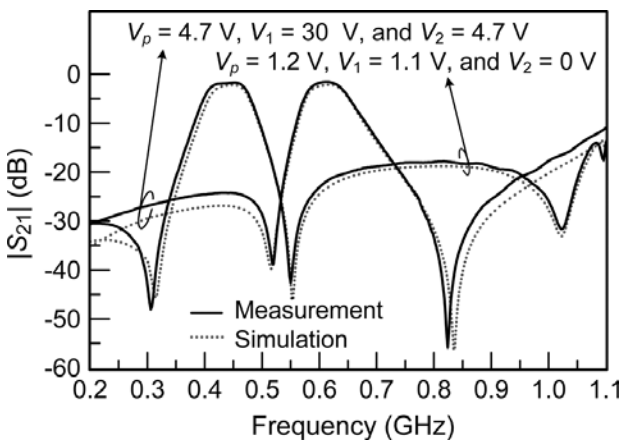

Fig. 14. Simulated and measured $|S_{21}|$ (dB) when $f_{bw} = 40$ MHz at f_c = 430 and 600 MHz.

The measured results consistent with the simulated ones (see Fig. 14) and the 1-dB (normalized) bandwidth is maintained at 55 ± 3 MHz. As for the passband bandwidth adjustment, Figs. 15 and 16 show the controllable f_{bw} of the filter with the center frequency located at 430 and 600 MHz, respectively. In both figures, the center frequency remains almost unchanged while the 1-dB bandwidth varies from 16 to 55 MHz. As f_{bw} decreases, the insertion loss (*IL*) increases from 1.4 to 4.45 dB for the case of the center frequency at 430 MHz while the *IL* increases from 1.63 to 4.63 dB for the case of the center frequency at 600 MHz. The increase of the *IL* is attributed to a decrease of the fractional bandwidth, as explained in [36]. Note that the 1-dB bandwidth of the filter can be further narrowed down to zero, as presented in Section II.

C. Filter Response Reconfigurability

The developed filter is capable of switching the quasi-elliptic passband response to the Chebyshev/Butterworth one via the removal of the transmission zeros, as demonstrated below. Fig. 17 shows the S-parameter data of the developed filter of a passband centered at 430 MHz with a 40-MHz f_{bw}. The solid lines correspond to the measured results of the filter of quasi-elliptic response while the dashed lines are the ones of the filter of Chebyshev response. As expected, the suppression of the transmission zeros at two band edges leads to higher out-of-band rejection. In addition, the simulated and measured results of the midband *IL* and the maximum 3-dB bandwidths with respect to f_c are presented in Fig. 18, where the solid and dashed lines, respectively, correspond to the quasi-elliptic and Chebyshev responses. On the other hand, owing to the tunable capability of the filter Q_{ext}

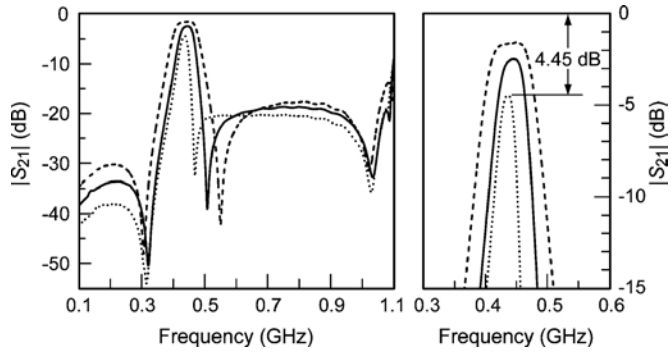

Fig. 15. Measured $|S_{21}|$ (in decibels) with f_{bw} adjustment at $f_c = 430$ MHz (dashed: $V_p = 1.2$ V, $V_1 = 1.1$ V, and $V_2 = 0$ V; solid: $V_p = 2.4$ V, $V_1 = 0.7$ V, and $V_2 = 0.1$ V; dotted: $V_p = 5$ V, $V_1 = 0.3$ V, and $V_2 = 0.1$ V).

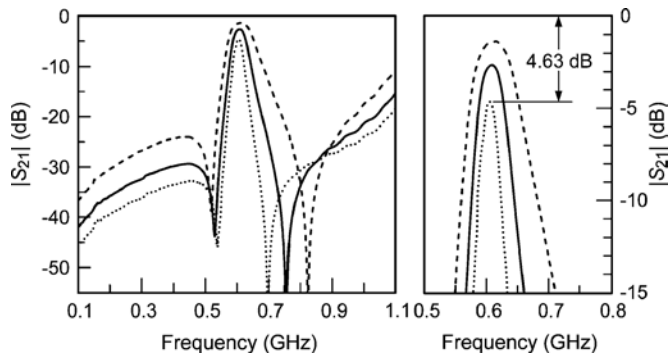

Fig. 16. Measured $|S_{21}|$ (in decibels) with f_{bw} adjustment $f_c = 600$ MHz (dashed: $V_p = 4.7$ V, $V_1 = 30$ V, and $V_2 = 4.7$ V; solid: $V_p = 8.6$ V, $V_1 = 15.6$ V, and $V_2 = 4.7$ V; dotted: $V_p = 15.4$ V, $V_1 = 11.6$ V, and $V_2 = 4.9$ V).

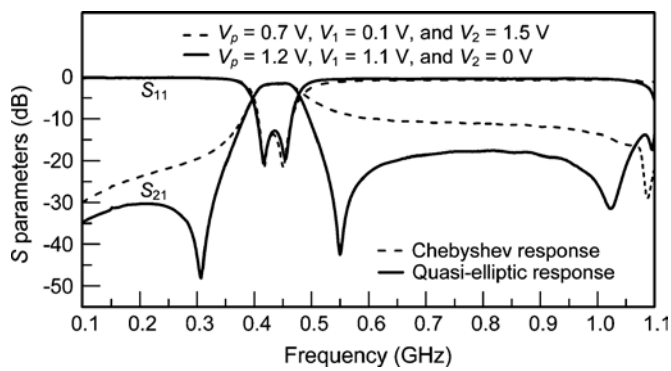

Fig. 17. Demonstration of the passband response switching from quasi-elliptic to Chebyshev.

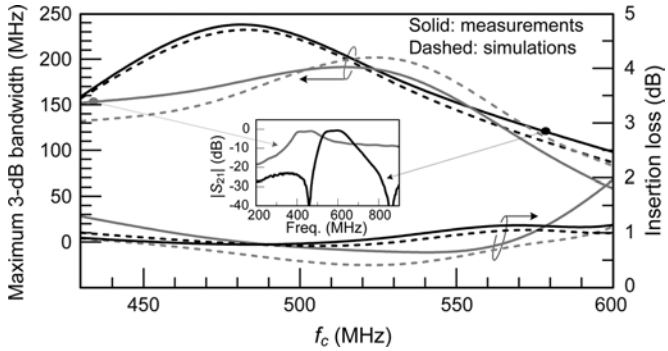

Fig. 18. Measured maximum 3-dB bandwidth and its corresponding *IL* with (black) or without (gray) transmission zeros as a function of f_c.

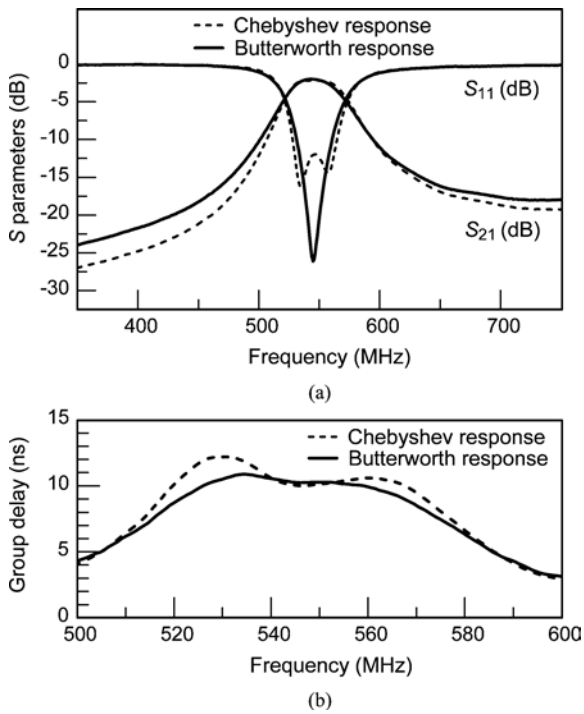

Fig. 19. Demonstration of the passband responses from Chebyshev to Butterworth. (a) S-parameter data. (b) Group delay. (Dashed: $V_p = 5.3$ V, $V_1 = 2.5$ V, $V_2 = 3.9$ V; solid: $V_p = 4.6$ V, $V_1 = 2.8$ V, $V_2 = 3.8$ V.)

and k, the filter passband of fixed f_c and f_{bw} is able to be reconfigured to different responses by a re-substitution of the corresponding g_n values. As shown in Fig. 19(a), f_c is selected as 550 MHz in which the Chebyshev response exhibits a higher selectivity, while the group delay for the Butterworth response has a flatter response within the passband, as observed in Fig. 19(b).

D. Switchable Passband Characteristics

Apart from the BPF applications, the constructed filter can also be used as an all-reject filter. For realization, the small k condition, i.e., $\tilde{f}_r^{even} \simeq \tilde{f}_r^{odd}$, is imposed to mimic the condition of $f_{bw} = 0$. As demonstrated in Fig. 20, a passband suppression greater than 24 dB over the entire fundamental frequencies is attained, and slight dissipated powers attributed from undesired

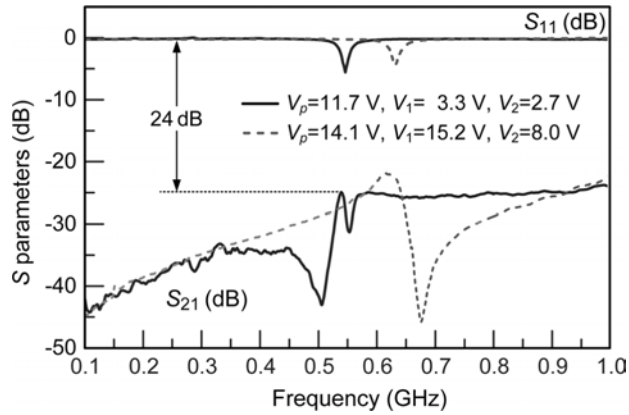

Fig. 20. Measurement passband response for all-reject operation.

TABLE II
MEASURED IIP_3, $IP_{1\mathrm{dB}}$, AND NF FOR DIFFERENT f_c AND f_{bw}

Experimental cases	f_c (MHz)	f_{bw} (MHz)	IIP_3, $IP_{1\mathrm{dB}}$ (dBm)	NF (dB) [uncertainty]
(i)	430	40	22.8 / 13.6	3.78 [±1.13]
(i)	480	40	21.6 / 15.1	3.83 [±1.12]
(i)	530	40	23.9 / >23	3.87 [±1.10]
(i)	570	40	24.5 / >23	4.03 [±1.08]
(i) and (ii)	600	40	26.1 / >23	4.34 [±1.02]
(ii)	600	25	25.4 / >23	4.48 [±1.07]
(ii)	600	12	26.3 / >23	6.06 [±1.12]

losses resulted in a nonzero $|S_{11}|$ (in decibels) can be observed at each frequency.

E. Filter Nonlinearity, Power Handling, and NF

The measurement on nonlinearity, power-handling capability, and noise performance of the constructed filter is carried out using a 50-Ω system. The nonlinearity is investigated by measuring the inter-modulation products at the filter output using a two-tone setup with frequencies separated by 0.1 MHz. As for the power-handling capacity, one-tone testing signal is injected into the filter with the power level varying from -5 to 23 dBm. The noise figure (NF) measurement is completed using Agilent E4446A PSA together with the noise source 346C at room temperature. Two measurement scenarios are performed and described as follows. The first scenario investigates the BPF of $f_{bw} = 40$ MHz and f_c is tuned from 430 to 600 MHz. The second one examines the BPF with $f_c = 600$ MHz and f_{bw} varies from 12 to 40 MHz. The passband $|S_{11}| = -15$ dB is also specified for both measurements. As tabulated in Table II, both cases have IIP_3's great than 20 dB. On the other hand, the $IP_{1\mathrm{dB}}$ increases as f_c increases since a higher bias voltage is required to reduce the varactor capacitance for an up-shift of f_c [4]. As for the noise performances, NF (in decibels) $\approx IL$ (in decibels) $+2 \pm 1.1$ is observed for all the cases, and the uncertainties are estimated by the tool provided.[1] Finally, the comparison of this filter with related works is summarized in Table III. The tuning range of f_c is obtained with the percentage

[1][Online]. Available: http://sa.tm.agilent.com/noisefigure/NFUcalc.html

TABLE III
MEASURED PERFORMANCE OF THE DEMONSTRATED FILTER AND COMPARISON WITH THE LITERATURE

	Filter type	f_c (MHz) {tuning range(%)}	f_{bw} (MHz) {ratio}	TZs (numbers)	IL, NF (dB)	IIP_3, $IP_{1\text{dB}}$ (dBm)	Types of Resonator (order)
[13]	I	8920-9870 {10.1}	359±25 MHz	2	>3.2, NA	NA	Modified square patch (2)#
[20]	I	1900-2350 {21.2}	Fixed at 5.75%	2	>2.1, NA	NA	Loop resonator (2)#
[21]	I	600-1030 {52.7}	85±5 MHz	1	>1.8, NA	NA	Open loop resonator (2)#
[28]*	III	2900-3500 {18.8}	4-12% {3}	0 or 2	>1.0, NA	>29.9, >14.5	Triangular patch (2)#
[29]	III	1630-1880 {14.2}	190-280 {1.47}	2	>2.4, NA	NA	Circular ring resonator (2)#
[26]	III	1500-2200 {37.8}	50-170 {3.4}	2	>3.0, NA	>11, <5	Comblines (3)
[27]	III	2000-2600 {26.1}	157-598 {3.8}	2	>1.4, NA	>15, NA	Active microstrip filter (2)
[31]	III	1500-2100 {30.1}	40-120 {3}	2	>4.5, NA	>5.5, <8	Comblines (4)
This work*◇	III	430-600 {33.0}	0-52	0 or 2	>0.7, IL+2±1.1	>21.6, >13.6	Loop resonator (2)#

TZ: transmisson zero; *: Filter with switchable passband capability ([28]: 11 dB rejection, this work: 24 dB rejection); ◇: Filter with reconfigurable passband response; #: dual-mode resonator.

of the ratio of the tuning range to the average f_c, and the major improvements are footnoted at the bottom of Table III.

IV. CONCLUSION

An effective approach for the development of microwave BPFs with high-frequency tuning capability has been presented. The approach exploits the dual-mode resonance associated with the loop-shaped resonator, and the even- and odd-mode resonant frequencies are able to be separately located predominately via the resonator form factor and altered with the incorporated varactor diodes. On the other hand, it has been shown that the tapped capacitor is critical to the accurate control of the passband response and its value determination is addressed. The effectiveness of the proposed approach has been experimentally demonstrated with the microstrip BPF of an up to 33% center frequency tuning range, an excellent bandwidth tuning capability, as well as a passband response reconfigurability. Specifically, the filter response can be reconfigured to be the Chebyshev, quasi-elliptic, or Butterworth functions for specified f_c and f_{bw}. For quasi-elliptic response, the zeros provide sharp skirts near the passband edges. Besides, the presented filter also offers a switchable characteristic with a suppression level greater than 24 dB. Owing to its various reconfigurable states, the proposed filter is expected to find applications in future communication systems.

ACKNOWLEDGMENT

The authors would like to thank Agilent Technologies, Taipei, Taiwan, for their helpful assistances; B.-C. Huang and B.-Z. Chow, both with the Graduate Institute of Communication Engineering, Yuan Ze University (YZU), Jhongli, Taiwan, for their valuable discussions and technical support; T.-J. Huang, H.-J. Jhang, and C.-Y. Chiang, all with YZU, for their instrument assistances; and Y.-T. Lo and Dr. S.-H. Yang, both with the Graduate Institute of Communication Engineering, National Taiwan University, Taipei, Taiwan, for their helpful suggestions.

REFERENCES

[1] M. Sherman, A. N. Mody, R. Martinez, and C. Rodriguez, "IEEE standards supporting cognitive radio and networks, dynamic spectrum access, and coexistence," *IEEE Commun. Mag.*, vol. 46, no. 7, pp. 72–79, Jul. 2008.

[2] B. Perlman, J. Laskar, and K. Lim, "Fine-tuning commercial and military radio design," *IEEE Microw. Mag.*, vol. 9, no. 4, pp. 95–106, Aug. 2008.

[3] J.-S. Fu and A. Mortazawi, "Improving power amplifier efficiency and linearity using a dynamically controlled tunable matching network," *IEEE Trans. Microw. Theory Techn.*, vol. 56, no. 12, pp. 3239–3244, Dec. 2008.

[4] H. M. Nemati, C. Fager, U. Gustavsson, R. Jos, and H. Zirath, "Design of varactor-based tunable matching networks for dynamic load modulation of high power amplifiers," *IEEE Trans. Microw. Theory Techn.*, vol. 57, no. 5, pp. 1110–1118, May 2009.

[5] M.-I. Lai, T.-Y. Wu, J.-C. Hsieh, C.-H. Wang, and S.-K. Jeng, "Design of reconfigurable antennas based on an L-shaped slot and PIN diodes for compact wireless devices," *IET Microw., Antennas, Propag.*, vol. 3, no. 1, pp. 47–54, Feb. 2009.

[6] C.-C. Huang, N.-W. Chen, H.-J. Tsai, and J.-Y. Chen, "A coplanar waveguide bandwidth-tunable low-pass filter with broadband rejection," *IEEE Microw. Wireless Compon. Lett.*, vol. 23, no. 3, pp. 134–136, Mar. 2013.

[7] W.-D. Yan and R. R. Mansour, "Tunable dielectric resonator bandpass filter with embedded MEMS tuning elements," *IEEE Trans. Microw. Theory Techn.*, vol. 55, no. 1, pp. 154–160, Jan. 2007.

[8] S. Yonghyun, W. Zhengzheng, and M. Rais-Zadeh, "A high-performance continuously tunable mems bandpass filter at 1 GHz," *IEEE Trans. Microw. Theory Techn.*, vol. 60, no. 8, pp. 2439–2447, Aug. 2012.

[9] J. Nath, D. Ghosh, J. P. Maria, A. I. Kingon, W. Fathelbab, P. D. Franzon, and M. B. Steer, "An electronically tunable microstrip bandpass filter using thin-film barium–strontium–titante (BST) varactors," *IEEE Trans. Microw. Theory Techn.*, vol. 53, no. 9, pp. 2707–2712, Sep. 2005.

[10] H. Jiang, B. Lacroix, K. Choi, Y. Wang, A. T. Hunt, and J. Papapolymerou, "Ka-and U-band tunable bandpass filters using ferroelectric capacitors," *IEEE Trans. Microw. Theory Techn.*, vol. 59, no. 12, pp. 3068–3074, Dec. 2011.

[11] L. H. Hsieh and K. Chang, "Tunable microstrip bandpass filters with two transmission zeros," *IEEE Trans. Microw. Theory Techn.*, vol. 51, no. 2, pp. 520–525, Feb. 2003.

[12] T.-Y. Yun and K. Chang, "Piezoelectric-transducer-controlled tunable microwave circuits," *IEEE Trans. Microw. Theory Techn.*, vol. 50, no. 5, pp. 1303–1310, May 2002.

[13] C. Lugo and J. Papapolymerou, "Dual-mode reconfigurable filter with asymmetrical transmission zeros and center frequency control," *IEEE Microw. Wireless Compon. Lett.*, vol. 16, no. 9, pp. 499–501, Sep. 2006.

[14] P. W. Wong and I. C. Hunter, "Electronically tunable filters," *IEEE Microw. Mag.*, vol. 10, no. 6, pp. 46–54, Oct. 2009.

[15] W.-H. Tu, "Compact low-loss reconfigurable bandpass filter with switchable bandwidth," *IEEE Microw. Wireless Compon. Lett.*, vol. 20, no. 4, pp. 208–210, Apr. 2010.

[16] C. H. Kim and K. Chang, "Ring resonator bandpass filter with switchable bandwidth using stepped-impedance stubs," *IEEE Trans. Microw. Theory Techn.*, vol. 58, no. 12, pp. 3936–3944, Dec. 2010.

[17] A. Miller and J.-S. Hong, "Cascaded coupled line filter with reconfigurable bandwidths using LCP multilayer circuit technology," *IEEE Trans. Microw. Theory Techn.*, vol. 60, no. 6, pp. 1577–1586, Jun. 2012.
[18] H.-J. Tsai, N.-W. Chen, and S.-K. Jeng, "Reconfigurable bandpass filter with separately relocatable passband edge," *IEEE Microw. Wireless Compon. Lett.*, vol. 22, no. 11, pp. 559–561, Nov. 2012.
[19] X.-G. Wang, X.-H. Cho, and S.-W. Yun, "A tunable combline bandpass filter loaded with series resonator," *IEEE Trans. Microw. Theory Techn.*, vol. 60, no. 6, pp. 1569–1576, Jun. 2012.
[20] E. E. Djoumessi, M. Chaker, and K. Wu, "Varactor-tuned dual-mode bandpass filter for wireless applications," in *IEEE Radio Wireless Symp.*, San Diego, CA, USA, Jan. 18–22, 2009, pp. 646–649.
[21] W. Tang and J.-S. Hong, "Varactor-tuned dual-mode bandpass filters," *IEEE Trans. Microw. Theory Techn.*, vol. 58, no. 8, pp. 2213–2219, Aug. 2010.
[22] S.-J. Park and G. M. Rebeiz, "Low-loss two-pole tunable filters with three different predefined bandwidth characteristics," *IEEE Trans. Microw. Theory Techn.*, vol. 56, no. 5, pp. 1137–1148, May 2008.
[23] X. Y. Zhang, Q. Xue, C. H. Chan, and B.-J. Hu, "Low-loss frequency-agile bandpass filters with controllable bandwidth and suppressed second harmonic," *IEEE Trans. Microw. Theory Techn.*, vol. 58, no. 6, pp. 1557–1564, Jun. 2010.
[24] M. A. El-Tanani and G. M. Reibez, "A two-pole two-zero tunable filter with improved linearity," *IEEE Trans. Microw. Theory Techn.*, vol. 57, no. 4, pp. 830–839, Apr. 2009.
[25] M. Sánchez-Renedo, R. Gómez-García, J. I. Alonso, and C. Briso-Rodríguez, "Tunable combline filter with continuous control of center frequency and bandwidth," *IEEE Trans. Microw. Theory Techn.*, vol. 53, no. 1, pp. 191–199, Jan. 2005.
[26] Y.-C. Chiou and G. M. Reibez, "A tunable three-pole 1.5–2.2-GHz bandpass filter with bandwidth and transmission zero control," *IEEE Trans. Microw. Theory Techn.*, vol. 59, no. 11, pp. 2872–2878, Nov. 2011.
[27] H.-I. Baek, Y.-H. Cho, X.-G. Wang, H.-M. Lee, and S.-W. Yun, "Design of a reconfigurable active bandpass filter based on a controllable slope parameter," *IEEE Microw. Wireless Compon. Lett.*, vol. 21, no. 12, pp. 670–672, Dec. 2011.
[28] A. L. C. Serrano, F. S. Correra, T.-P. Vuong, and P. Ferrari, "Synthesis methodology applied to a tunable patch filter with independent frequency and bandwidth control," *IEEE Trans. Microw. Theory Techn.*, vol. 60, no. 3, pp. 484–493, Mar. 2012.
[29] M.-F. Lei and H. Wang, "An analysis of miniaturized dual-mode bandpass filter structure using shunt-capacitance perturbation," *IEEE Trans. Microw. Theory Techn.*, vol. 53, no. 6, pp. 861–867, Mar. 2005.
[30] T. S. Beukman and R. H. Geschke, "A tune-all wideband filter based on perturbed ring-resonators," *IEEE Microw. Wireless Compon. Lett.*, vol. 23, no. 3, pp. 131–133, Mar. 2013.
[31] Y.-C. Chiou and G. M. Rebeiz, "Tunable 1.55-2.1 GHz 4-pole elliptic bandpass filter with bandwidth control and $>$50 dB rejection for wireless systems," *IEEE Trans. Microw. Theory Techn.*, vol. 61, no. 1, pp. 117–124, Jan. 2013.
[32] J.-S. Hong, "Reconfigurable planar filters," *IEEE Microw. Mag.*, vol. 10, no. 6, pp. 75–83, Oct. 2009.
[33] I. Wolff, "Microstrip bandpass filter using degenrate modes of a microstrip ring resonator," *Electron. Lett.*, vol. 8, no. 12, pp. 302–303, 1972.
[34] M. Guglielmi and G. Gatti, "Experimental investigation of dual-mode microstrip ring resonators," in *20th Eur. Microw. Conf.*, 1990, pp. 901–906.
[35] S.-F. Chao, C.-H. Wu, Z.-M. Tsai, H. Wang, and C.-H. Chen, "Electronically switchable bandpass filters using loaded stepped-impedance resonators," *IEEE Trans. Microw. Theory Techn.*, vol. 54, no. 12, pp. 4193–4201, Dec. 2006.
[36] J. S. Hong and M. J. Lancaster, *Microstrip Filters for RF/Microwave Applications*. New York, NY, USA: Wiley, 2001.
[37] M. Makimoto and S. Yamashita, *Microwave Resonators and Filters for Wireless Communication: Theory, Design and Application*. Berlin, Germany: Springer-Verlag, 2000.
[38] B. T. Tan, S. T. Chew, M. S. Leong, and B. L. Ooi, "A dual-mode bandpass filter with enhanced capacitive perturbation," *IEEE Trans. Microw. Theory Techn.*, vol. 51, no. 8, pp. 1906–1910, Aug. 2003.
[39] L.-K. Yeung, K.-L. Wu, and Y.-E. Wang, "Low-temperature cofired ceramic LC filters for RF applications," *IEEE Microw. Mag.*, vol. 9, no. 5, pp. 118–128, Oct. 2008.
[40] K. Buisman, L. C. N. de Vreede, L. E. Larson, M. Spirito, A. Akhnoukh, T. L. M. Scholtes, and L. K. Nanver, "Distortion-free varactor diode topologies for RF adaptivity," in *IEEE MTT-S Int. Microw. Symp. Dig.*, Long Beach, CA, USA, Jun. 12–17, 2005, pp. 157–160.
[41] C. Huang, K. Buisman, L. K. Nanver, F. Sarubbi, M. Popadić, T. L. M. Scholtes, H. Schellevis, L. E. Larson, and L. C. N. de Vreede, "A 67 dBm OIP_3 multistacked junction varactor," *IEEE Microw. Wireless Compon. Lett.*, vol. 18, no. 11, pp. 749–751, Nov. 2008.
[42] "Silicon abrupt junction varactors," Skyworks Solutions Inc., Santa Clara, CA, USA, Data Sheet SMV1405-SMV1430 Series: Plastic Packaged Abrupt Junction Tuning Varactors, Mar. 2013.
[43] "Silicon abrupt junction varactors," Skyworks Solutions Inc., Santa Clara, CA, USA, Data Sheet SMV1231-SMV1237: Hyperabrupt Tuning Varactors, Jun. 2012.

Hsuan-Ju Tsai (S'12) was born in Taoyuan, Taiwan. He received the B.E. degree in mechatronic technology from National Taiwan Normal University (NTNU), Taipei, Taiwan, in 2008, the M.S.E.E. degree in electrical engineering from National Central University (NCU), Taoyuan, Taiwan, in 2010, and is currently working toward the Ph.D. degree at National Taiwan University (NTU), Taipei, Taiwan.

Since December 2011, he has been a Research Assistant of communications engineering with Yuan Ze University, Jhongli, Taiwan. He is currently a technical consultant for *FHM Magazine Taiwan* for introducing some novel electromagnetic applications. He holds two U.S. patents and two Taiwan patents, all related to ultra-fast optoelectronic devices. His research interests include the design and analysis of microwave/millimeter-wave (MMW) circuits, MMW antennas, and ultrahigh-speed photonics and their applications to communication.

Mr. Tsai has been a reviewer for the IEEE TRANSACTIONS ON MICROWAVE THEORY AND TECHNIQUES.

Nan-Wei Chen (M'03) received the B.S. degree in atmospheric sciences and M.S. degree in space sciences from National Central University, Jhongli, Taiwan, in 1993 and 1995, respectively, and the Ph.D. degree in electrical engineering from the University of Illinois at Urbana-Champaign, Urbana, IL, USA, in 2004.

From 1998 to 2004, he was a Research Assistant with the Center for Computational Electromagnetics, University of Illinois at Urbana-Champaign, where he was involved with time-domain integral-equation methods for the solution of scattering and radiation problems. From 2004 to 2009, he was an Assistant Professor of electrical engineering with National Central University, Taoyuan, Taiwan. Since 2010, he has been an Associate Professor of communications engineering with Yuan Ze University, Jhongli, Taiwan. His research interests include computational electromagnetics with a special emphasis on time-domain integral equations, periodic structures, and millimeter-wave antennas and passive circuits.

Dr. Chen was the recipient of the 2004 Raj Mittra Outstanding Research Award from the University of Illinois at Urbana-Champaign and the 2010 Best Article Award from the Chinese Geoscience Union.

Shyh-Kang Jeng (M'86–SM'98) received the B.S.E.E. and Ph.D. degrees from National Taiwan University, Taipei, Taiwan, in 1979 and 1983, respectively.

In 1981, he joined the faculty of the Department of Electrical Engineering, National Taiwan University, where he is currently a Professor. From 1985 to 1993, he was a Visiting Research Associate Professor and a Visiting Research Professor with the University of Illinois at Urbana-Champaign. In 1999, for six months, he visited the Center for Computer Research in Music and Acoustics, Stanford University, Stanford, CA, USA. His research interest includes time-domain electromagnetic field computation techniques, antenna design, multimedia signal processing, computational neuroscience, and computational cognitive neuroscience.

Dr. Jeng was a recipient of the 1998 Outstanding Research Award of the National Science Council and the 2004 Outstanding Teaching Award of National Taiwan University.